Design and Optimization of Segmental Translator Linear Switched Reluctance Motor

Milad Golzarzadeh[a*], Hashem Oraee[a], Babak Ganji[b]

1- Milad Golzarzadeh

E-mail: milad.golzarzadeh@ee.sharif.edu

2- Hashem Oraee

E-mail: oraee@sharif.edu

3- Babak Ganji

E-mail: bganji@kashanu.ac.ir

a) Department of Electrical Engineering, Sharif University of Technology, Tehran, Iran

b) Faculty of Electrical and Computer Engineering, University of Kashan, Kashan, Iran

---

[*]Corresponding author: Milad Golzarzadeh

E-mail: milad.golzarzadeh@ee.sharif.edu

Abstract: Due to the special design of the segmental translator linear switched reluctance motor (STLSRM), it has a higher power density than conventional linear switched reluctance motor (LSRM). Having enough information about the parameters affecting the motor output can help to improve its performance. In this paper, a step-by-step and integrated method is presented for the standard design of STLSRM. After obtaining the design equations, the important and effective parameters on the STLSRM performance are determined and discussed. Using sensitivity analysis, design considerations and comprehensive instructions are provided to determine the STLSRM dimensions. In order to confirm the design process, a typical STLSRM is designed for the use of electric sliding doors, and with the goal of increasing the average instantaneous thrust force and reducing the force ripple, based on the design of experiments (DOE) approach and the response surface method (RSM), the optimization of STLSRM is done. In order to validate, using the finite element method (FEM), the performance characteristics of the optimized STLSRM including flux-linkage, co-energy, static force, instantaneous thrust force waveform and instantaneous current waveform are compared with those of derived from the initial design.

Keywords: *Switched Reluctance Motor, Segmental Translator, Sensitivity Analysis, Design of Experiments, Finite Element Method.*

1. Introduction

Switched reluctance motors (SRMs) have features such as simple structure, robustness, use in harsh environments, low maintenance cost, and the existence of windings on only one-side [1-3]. In the SRM the windings have independent functions and mutual inductance that occurs between the two phases is very small and can be ignored, so that if one phase is damaged, it does not have a destructive effect on the other phases. Therefore, fault tolerance and high reliability are other features of SRM. Due to these inherent characteristics, the SRMs are used in many applications [3-6].

SRMs are divided into two categories: rotary and linear. The LSRMs have the same structure and performance as its rotary type, with the difference that they have linear displacement instead of rotary motion. Therefore, they have the advantages of rotary SRMs. LSRMs have two types, one-side and dual-side, which, unlike rotary motors, are used in many horizontal and vertical applications without the need for any converter to convert motion [7-10]. Many researchers have investigated different structures of LSRMs and various researches have been carried out on different aspects of LSRMs and special linear motors have been designed to improve their performance [11-15]. In [16], a standard design method with good accuracy for LSRM is presented. This design is first performed in the domain of rotary SRM, then it is brought to the linear domain by performing appropriate transformations, which increases the volume of calculations.

One of the special structures is the design of stator/translator in the LSRM without a yoke, which instead of using prominent poles in the stator/translator, discrete segments are used. In conventional LSRM, the stator yoke and the translator yoke make up most of the core volume, which is a path for the flux to pass from one tooth to another tooth. Therefore, yoke does not increase the carrying flux does not increase the ability to carry the flux, and due to large volume of yoke, the use of magnetic materials increases, which leads to a decrease in power density. To solve this defect, in [17-19], double-sided LSRMs with segmental stator have been designed, analyzed and optimized, which significantly increases the power density due to the removal of yoke in the stator. In these motors, the windings are usually located on the moving part, which reduces the reliability and increases the maintenance cost due to the displacement of winding by the moving part. To solve this problem, a special type of linear switched reluctance motors (STLSRM) is presented in [20-21], in which the translator does not have a yoke, and instead of using connected poles, separate segments are used. In this structure, the volume of magnetic materials is reduced due to the absence of yoke in the

translator, which increases the power density, and due to the fact that the windings are located on the stationary part and the moving part is isolated from the electric current and permanent magnet, the maintenance cost is low and the reliability is increased [22-23]. Also, in other electric motors, such as the flux-switching linear motor, which works in some principles like the linear switched reluctance motor, the absence of a yoke and the use of discrete segments have improved the performance of the motor [24].

According to the literature review, although various linear motors have been introduced in which the yoke is removed and many researches have been carried out on their various aspects including dimensional design, electromagnetic design and thermal design, for the STLSRM presented in this paper, the design equations of motor dimensions have not yet been presented. In addition, the important novelty of this research is the design and optimization of STLSRM for the use of electric sliding doors, because unlike segmental linear motors where the coils are on the translator, in the STLSRM, the coils are on the stationary part and the translator is isolated from the electric current. Therefore, this motor can be used appropriately in short distances. Choosing the right method for design is important because it allows the designer to directly observe and analyze the design parameters and increase the design speed with good accuracy. Therefore, in this paper, an integrated and step-by-step design method is presented considering the specific design aspects for the STLSRM. This design process is done directly in the linear motor domain without converting to the rotary motor domain. As a result, it gives the designer high flexibility to choose key parameters and motor dimensions. Using sensitivity analysis, the effect of motor geometric parameters on its performance is discussed, then detailed and comprehensive guidelines are provided for determining the dimensions of STLSRM using the FEM. After obtaining the design equations and carrying out sensitivity analysis to determine the dimensions of motor, a STLSRM is designed for the use of electric sliding doors, and with the goal of reducing the force ripple and increasing the average instantaneous thrust force, the optimization of STLSRM is done based on the DOE approach and the RSM.

Based on this, the STLSRM is introduced in section 2, and in section 3, the design of this motor is carried out in the linear domain and the design equations are given in detail, then in section 4, sensitivity analysis is performed to investigate the effect of geometric dimensions on the performance of the motor. In section 5, the design of STLSRM for the use of electric sliding doors is carried out, and with the goal of increasing the average instantaneous thrust force and reducing the force ripple, the motor optimization is done in section 6. In order to

validate the research, the simulation results are given in Section 7. Finally, in section 8, a summary and conclusion for this paper is given.

2. Configuration of STLSRM

The cross-section and three-dimensional geometry of the three-phase STLSRM are shown in Fig. 1. Each slot of the stator is filled with one phase winding, and the winding of each phase includes three poles of stator. The translator consists of a set of ferromagnetic segments that are magnetically and mechanically separated from each other. The ferromagnetic segments are placed on the non-magnetic part so that no flux path is created between the segments in the aligned position. Therefore, a structure is created with several independent parts that are similar in principles and performance. Unlike the conventional LSRM in which the flux lines pass through the stator yoke and the translator yoke and close their path through the teeth of stator and translator, in the STLSRM, the generated flux follows an almost circular path around two adjacent teeth of the stator, which causes the length of magnetic flux path to be shorter. Therefore, due to the unusual structure of the STLSRM, the design process of this motor cannot be easily done in the rotary domain and is done directly in the linear domain.

Flux lines in aligned and unaligned positions for the STLSRM, with excitation of phase B, are drawn by ANSYS software and shown in Fig. 2. In this motor, the flux produced by winding of different phases in the position of aligned closes its path through a segment of the moving part and does not disperse between similar segments. Each flux path can be considered as a power generation section that is independent from other sections in terms of magnetic circuit structure and similar to other sections in terms of operation. Therefore, each power generation section can be considered as a STLSRM, which provides a high degree of flexibility for motor design. Like rotary SRMs, in conventional LSRMs, most of the core volume is made up of the stator and translator yokes, which are a path for the flux to pass from one tooth to another. Therefore, the stator yoke and rotor yoke do not increase the flux carrying capacity. Because the yoke comprises most of the volume and weight of the core, the use of magnetic materials increases, which leads to a decrease in power density. To solve this defect, the power density has been increased in the STLSRM by reducing the active magnetic materials. Therefore, instead of the poles connected to the yoke, discrete segments have been used in the moving part. This change has removed the yoke from the moving part, which significantly increases the power density in this motor. The prominent advantages of the STLSRM are summarized as follows:

- The moving part does not have a yoke. Therefore, the use of magnetic core material is significantly reduced.
- The ferromagnetic segments of the moving part are placed on non-magnetic steel, and the gap between them can be filled with non-magnetic materials. Therefore, due to the absence of tooth and slot in the secondary, there is no windage loss in the running part.
- Each slot is completely filled with only one phase winding. Therefore, the use of insulating materials in the stator slot decreases and its space coefficient increases, which increases the output power.
- Due to the absence of an insulating separator in the stator slot, the surface of slot is optimally used and facilitates the manufacturing process.
- The winding of each stator slot produces flux independently, which is separate from the flux produced by the coil of other phases.
- Due to the absence of yoke in the moving part, iron losses are reduced.
- The flux produced by the coil of different phases closes its path through a segment that is separate from other segments of the moving part and causes the flux produced by the phases not to be dispersed between similar parts. Therefore, each flux generating section can be considered as an independent STLSRM, which gives the designer considerable flexibility.

3. Integrated Design of STLSRM

Because the STLSRM is characterized by a unique magnetic circuit and independent power generation parts, it has a different design compared to the conventional LSRM. Therefore, here an integrated design method considering specific aspects for STLSRM is presented. This design process is carried out directly in the domain of linear motor without converting to the domain of rotary motor. The special parameters required for design of motor are shown in Fig. 3.

The presented motor has an axial length of L_{stk} and a maximum linear speed of V_{m}, which reaches the maximum speed from the stationary state in the period of time t_a. If the maximum mass of the moving part, the maximum acceleration and the instantaneous acceleration force are expressed by M_{tr}, a_{tr} and F_{tr} respectively, the maximum acceleration and the instantaneous acceleration force are calculated from (1) and (2), respectively [25].

$$a_{tr} = \frac{V_m}{t_a} \tag{1}$$

$$F_{tr} = M_{tr} a_{tr} \tag{2}$$

Ignoring the friction force, the maximum output power of motor (P_o) is equal to:

$$P_o = F_{tr} V_m \tag{3}$$

The first step in the design of electric motors is to find the output (dimensional) equation that describes the relationship between the output power, speed, dimensions, and specific electric and magnetic loads of the motor. The output power of motor can be rewritten according to the input parameters of machine, i.e., voltage and current of the input terminal. If P_{in} and η are the input power and efficiency of the motor, respectively, the following equation can be written:

$$P_o = \eta P_{in} \tag{4}$$

If the input voltage and current of each phase are denoted by e and i respectively, (4) can be rewritten as (5):

$$P_o = \eta e i \tag{5}$$

Ignoring the voltage drop of the coil resistance, the voltage of each phase is obtained from the following equation:

$$e = \frac{d\lambda}{dt} \tag{6}$$

where λ is the flux-linkage of winding. The changes of winding flux-linkage during a period of time Δt, which includes the movement of moving part from the aligned position to unaligned position, is calculated by (7).

$$\Delta\lambda = \lambda_a - \lambda_u = e\Delta t \tag{7}$$

In the $\lambda - i$ characteristic, for simplicity, its nonlinear part can be omitted. Therefore, the changes of flux-linkage are expressed by the following equation:

$$\Delta\lambda = \Delta L i = (L_a - L_u) i \tag{8}$$

where L_a and L_u are the phase inductance in aligned and unaligned positions, respectively. If τ_{tr} is the pole pitch of moving part and τ_s is the pole pitch of stator, they are calculated from the following equations according to Fig. 3:

$$\tau_{tr} = W_{tr} + W_{so} = 2W_{sp} + 2W_{so} = 2(W_{sp} + W_{so}) \tag{9}$$

$$\tau_s = W_{tsp} + W_{so} = W_{sp} + W_{ss} \tag{10}$$

If Δx_{tr} is the distance between the aligned and unaligned positions, the duration of the movement of moving part is obtained from the following equations:

$$\Delta x_{tr} = V_m \Delta t \tag{11}$$

$$\Delta x_{tr} = W_{sp} + W_{so} = \frac{\tau_{tr}}{2} \tag{12}$$

From (11) and (12), the following equation can be written:

$$\Delta t = \frac{\tau_{tr}}{2V_m} \tag{13}$$

From (7), (8) and (13), the following equation is obtained:

$$(L_a - L_u)i = e\frac{\tau_{tr}}{2V_m} \tag{14}$$

Therefore, the input terminal voltage (e) is calculated from the following equation:

$$e = \frac{2V_m i(L_a - L_u)}{\tau_{tr}} = \frac{2V_m L_a i(1 - \frac{L_u}{L_a})}{\tau_{tr}} \tag{15}$$

If it is assumed that $k_1 = \frac{L_u}{L_a}$, equation of (15) is rewritten as follows:

$$e = \frac{2V_m L_a i(1-k_1)}{\tau_{tr}} = 2V_m \lambda_a \frac{(1-k_1)}{\tau_{tr}} \tag{16}$$

In the fully aligned position, assuming that the flux density in the air-gap and the flux density passing through the stator pole are equal, λ_a can be obtained from the following equation:

$$\lambda_a = NA_{ga}B_g \tag{17}$$

where N is the number of turns per phase, A_{ga} is the cross-sectional area of the flux passing through the air-gap and B_g is the flux density in the air-gap. The cross-sectional area of flux passing through the air-gap is calculated from the following equation:

$$A_{ga} = W_{ol} L_{stk} \tag{18}$$

where W_{ol} according to Fig. 3, is the overlapping width of translator and stator pole. From (17) and (18) the following equation is obtained:

$$\lambda_a = N W_{ol} L_{stk} B_g \tag{19}$$

The width of flux lines passing through the air-gap can be written in terms of the stator pole pitch as follows:

$$\tau_s = W_{sp} + W_{so} + 2W_{os} = W_{ol}\left(1 + \frac{W_{so} + 2W_{os}}{W_{ol}}\right) \tag{20}$$

If it is assumed that $k_2 = \frac{W_{so} + 2W_{os}}{W_{ol}} = \frac{W_{ss}}{W_{sp}}$, (20) is rewritten as follows:

$$W_{ol} = \frac{\tau_s}{1 + k_2} \tag{21}$$

From (19) and (21) we can write:

$$\lambda_a = N L_{stk} B_g \frac{\tau_s}{1 + k_2} \tag{22}$$

If ac is the specific electric load, it is calculated as follows [18]:

$$ac = \frac{Z_{ph} i}{L_s} \tag{23}$$

where Z_{ph} is the number of conductors of each phase and L_s is the length of stator. Because the winding includes a forward arm and a return arm, the number of conductors of each phase is twice the number of turns per phase. that's mean:

$$Z_{ph} = 2N \tag{24}$$

From (23) and (24) we can write:

$$ac = \frac{2Ni}{L_s} \tag{25}$$

It should be noted that in (25), the number of phases that are active simultaneously is considered equal to 1. From (5), (16) and (22), the output power equation (dimensional equation) is expressed as follows:

$$P_o = 2\eta V_m iNL_{stk} B_g \frac{1-k_1}{1+k_2} \frac{\tau_s}{\tau_{tr}} \quad (26)$$

From (26) and (25) we have:

$$P_o = \eta V_m acL_s L_{stk} B_g \frac{1-k_1}{1+k_2} \frac{\tau_s}{\tau_{tr}} \quad (27)$$

From (27) the axial length of the motor can be calculated. It should be noted that the ratio $\frac{\tau_s}{\tau_{tr}}$ can be written as the ratio of number of moving part segments to the number of stator poles, which is equal to 2/3 in this motor. Also, in this motor, the length of stator is equal to the length of moving part. Therefore, for a three-phase motor whose stator includes 6 poles, the stator length is obtained from the following equation:

$$L_s = 6W_{sp} + 6W_{ss} \quad (28)$$

To prevent oversaturation as well as uniform field distribution, the following design restrictions apply to this motor:

- The stator yoke height, the segment height of moving part and the stator pole width are equal.
- In the fully aligned position, the overlapping length of segment and the stator pole width are equal.
- The length of distance between the two segments of the moving part is equal to the slot opening of stator.

According to Ampere's law, the ampere-turn needed to produce the magnetic field intensity in air-gap is obtained from the following equation:

$$Ni = 2l_g H_g \quad (29)$$

where:

$$H_g = \frac{B_g}{\mu_0} \quad (30)$$

where l_g is the length of air-gap, H_g is the intensity of magnetic field in the air-gap, and μ_0 is the air magnetic permeability coefficient. Assuming the maximum phase current for the motor, the number of turns per phase is calculated from the following equation:

$$N = \frac{2 l_g B_g}{i \mu_0} \tag{31}$$

The cross-section area of conductors (a_c) is calculated from the following equation:

$$a_c = \frac{i}{\delta \sqrt{m}} \tag{32}$$

where δ is the maximum winding current density and m is the number of phases. The total cross-sectional area of the winding in one slot of stator is Na_c . If k_s is the space coefficient of stator slot, the area of each slot is obtained from the following equation:

$$a_s = \frac{Na_c}{k_s} \tag{33}$$

If h_{ss} is the height of stator slot, a_s is obtained from the following equation:

$$a_s = h_{ss} W_{ss} \tag{34}$$

where:

$$W_{ss} = W_{so} + 2W_{os} \tag{35}$$

Therefore, the stator slot height is calculated as follows:

$$h_{ss} = \frac{Na_c}{k_s W_{ss}} \tag{36}$$

In (36) k_s is usually considered a value between 0.2 and 0.7. Having the stator slot height, the stator tooth height (h_{sp}) is obtained as follows:

$$h_{sp} = h_{ss} + h_{st} \tag{37}$$

where h_{st} according to Fig. 3, is the height of stator pole shoe.

To select a specific electrical load, designers tend to choose it as large as possible, but there are limitations such as copper losses and temperature rise. Choosing a large value of ac leads to an increase in temperature and copper losses. Therefore, the cooling system used must be designed so that the temperature increase does not exceed the maximum temperature value determined by the insulation class used. The specific electrical load is considered equal to 25000 A/m. Dimensional equation (27) is obtained for a unit of STLSRM. If the length of stator is doubled and tripled, two and three units are created, respectively, which have independent functions.

If the number of independent units of the STLSRM is denoted by n_s, considering that each unit is capable of producing an independent linear force, the total force of motor can be expressed as follows:

$$F_t = n_s F_s \tag{38}$$

where F_t is the thrust force of all units and F_s is the thrust force for the one unit of STLSRM.

4. Sensitivity Analysis to Determine The Important Dimensions of STLSRM

The geometric dimensions of the motor have a significant effect on the inductance of aligned position, the inductance of unaligned position and thrust force. Therefore, after forming the dimensional equation and calculating the motor parameters, it is possible to consider the optimal design for the STLSRM by sensitivity analysis for the motor geometrical parameters. The stator pole width (W_{sp}), the stator slot width (W_{ss}), the translator segment width (W_{trb}) which depends on the segment angle (θ_{tr}), the height of stator pole shoe (h_{st}) and the length of air-gap between the stator and the translator (l_g) are the basic parameters for sensitivity analysis. It is important to have sufficient knowledge about the effect of these geometric quantities on machine performance. Therefore, to investigate the effects of key parameters using two-dimensional analysis and based on the FEM, the STLSRM simulation and the effect of geometrical parameters on the performance of motor, as well as instructions for determining the important dimensions of STLSRM are presented.

4.1. Stator slot width (W_{ss}) and stator pole width (W_{sp}):

The distance between the two adjacent poles of stator (the distance between two adjacent segments of translator), are effective in the flux distribution. With the increase of k_2, which is the ratio of the width of stator slot to the width of stator pole, this distance (W_{so}) increases. According to Fig. 4 a and c, in the aligned position, with the decrease W_{so}, the overlap area between the stator teeth and the moving part segments increases, and with the increase W_{so}, the overlap area between the stator poles and translator segments decreases. Also, according

to Fig. 4 b and d, in the unaligned position, the length of distance between the stator poles and translator segments decreases with the decrease of W_{so}, and the length of distance between the stator poles and translator segments increases with the increase of W_{so}. Therefore, with the increase of W_{so}, the inductance should decrease in the unaligned position, which seems to increase the power, but, at the same time, the inductance also decreases in the aligned position. As a result, it causes a decrease in the difference between co-energy in the positions of aligned and unaligned, which leads to a decrease in the motor's power output.

The curves of unaligned inductance, aligned inductance and their ratio (k_1) with changes of k_2 are shown in Fig. 5a. Also, the curve of average thrust force with changes of k_2 is given in Fig. 5b. As it is clearly seen in Fig. 5a, with the increase of k_2, unaligned inductance, aligned inductance and average thrust force decrease. According to the dimensional equation (27), the variables k_1 and k_2 are effective in the value of output power. that's mean:

$$P_o \propto \frac{1-k_1}{1+k_2} \tag{39}$$

According to (39), both the decrease of k_1 and the decrease of k_2 lead to an increase in force. But, as seen in Fig. 5a, the change value of k_1 is very small compared to k_2. Therefore, the effect of k_2 on the output power is much greater. That is, it is possible to obtain a higher power output by choosing a smaller k_2, although a large k_1 value is chosen. Considering that in the range of 0.6-0.8 there is a noticeable decrease in the value of alignment inductance and average thrust force, the appropriate choice is in the range of 0.8-1.1.

4.2. Bottom width of segment (W_{trb}):

Another important parameter is the bottom width of the segment trapezoidal geometry (W_{trb}) that according to Fig. 6 is dependent on the segment (θ_{tr}), and has an effect on the output power. The relationship between W_{trb} and θ_{tr} can be obtained using Fig. 6 as follows:

$$\tan\theta_{tr} = \frac{h_{tr}}{\delta_m} \tag{40}$$

The value of δ_m is uncertain and must be calculated through the relationship between the dimensions of segment and stator. From Fig. 3 and Fig. 6, the following equations are written:

$$2\delta_m + W_{trb} = 2W_{sp} + W_{so} \tag{41}$$

$$\tan\theta_{tr} = \frac{2h_{tr}}{2W_{sp} + W_{so} - W_{trb}} \tag{42}$$

It can be clearly seen that with the increase of θ_{tr}, the value of W_{trb} also increases. As shown in Fig. 7 a and b, the inductance in aligned position increases due to the large area that is created by increasing the value of θ_{tr}, which causes an increase in W_{trb} and the cross-sectional area of flux. At the same time, the large value of θ_{tr} leads to the increase of W_{trb} and the creation of a small gap between the two segments in the unaligned position, which increases the inductance in the unaligned position (Fig. 7 c and d).

Aligned inductance, unaligned inductance, their ratio (k_1) and the average thrust force with changes of θ_{tr} are obtained from the FEM and using ANSYS software, which can be seen in Fig. 8. The most appropriate value of θ_{tr} to produce the maximum driving force is from 45° to 75°, which is mainly due to the compromise between the maximum aligned inductance and the minimum unaligned inductance as shown in Fig. 8a.

4.3. Stator pole shoe height (h_{st}):

The height of stator pole shoe (h_{st}) also affects the performance of the STLSRM, which is considered as a percentage of stator tooth height. that's mean:

$$h_{st} = k_3 h_{sp} \tag{43}$$

where k_3 is a percentage of the stator tooth height, which is considered for the height of stator pole shoe. With the increase of k_3, the space of stator slot is reduced and the volume of stator teeth is increased. Aligned inductance, unaligned inductance, their ratio (k_1) and the average thrust force with changes of k_3 are obtained from the FEM, which can be seen in Fig. 9. With

the increase of k_3, the inductance of unaligned position, the inductance of aligned position and the average thrust force increase, which is due to the increase in the difference between the co-energy of the aligned and unaligned positions. According to Fig. 9a, for large k_3, the increasing speed of aligned inductance decreases, which leads to an increase of k_1. Therefore, according to Fig. 9b, the increasing speed of average thrust force also decreases and reaches a constant value. Considering that the increase of k_3 leads to the use of more magnetic materials and makes the geometry of stator slot space asymmetric, the design process becomes more difficult. Also, considering that the average thrust force has a small change rate after $k_3 = 0.15$, the appropriate choice for k_3 is between 0.15 and 0.45, and according to Fig. 9, $k_3 = 0.2$ is a good choice.

4.4. Air-gap length (l_g):

One of the most important design parameters is the air-gap between the stator and moving part, which has a great impact on the STLSRM performance. The curves of unaligned inductance, aligned inductance and their ratio with changes of l_g are shown in Fig. 10a. Also, the average thrust force curve with the changes of l_g is brought in Fig. 10b. As it is clearly seen in Fig. 10, with the increase of l_g, the inductance of unaligned position increases and the inductance of aligned position and the average thrust force decrease, which is due to the reduction of the difference between the co-energy of the aligned and unaligned positions. Therefore, considering the mechanical limitations, the appropriate choice for the length of air-gap is 0.5-1 mm.

Sensitivity analysis gives the designer a good initial insight into the effect of four geometrical parameters k_1, θ_{tr}, k_3 and l_g on inductance and thrust force. However, it is difficult to determine the exact value using the mathematical design method, and an optimization process can be applied to obtain the optimal values. However, the effect of these four parameters on STLSRM performance and their range of selection are stated in this section.

5. Design of A 3-Phase STLSRM for The Use of Electric Sliding Doors

After obtaining the design equations and sensitivity analysis to determine the approximate dimensions of the STLSRM, in this section, to confirm the design process, a STLSRM with the characteristics of maximum linear speed ($V_{\max}$) 0.5 m/s, maximum mass ($M_{\max}$) 62 kg and the acceleration time from stationary state to maximum speed (t_a) 0.5 seconds, is designed for the use of electric sliding doors. The acceleration of translator (a_{tr}) and the productive force (F_{tr}) are calculated as follows:

$$a_{tr} = \frac{V_{\max}}{t_a} = \frac{0.6}{0.5} = 1.2\, m/s^2 \tag{44}$$

$$F_{tr} = M_{\max} a_{tr} = 62 \times 1.2 = 74.4N \tag{45}$$

Having productive force, the maximum power is calculated as follows:

$$P_o = F_{tr} V_{\max} = 74.4 \times 0.6 \approx 45W \tag{46}$$

Considering the air-gap length 1 mm, the air-gap flux density 1.1 T, and the peak current 10 A for each phase, the number of turns per phase is obtained from the following equation:

$$N = \frac{2 l_g B_g}{i \mu_0} = \frac{2 \times 1 \times 10^{-3} \times 1.1}{10 \times 4\pi \times 10^{-7}} \approx 175 \tag{47}$$

The maximum allowable current density of the winding $\delta = 6\, A/mm^2$ and the number of phases $m = 3$ are considered. Therefore, the cross-sectional area of conductors (a_c) is calculated as follows:

$$a_c = \frac{i}{\delta \sqrt{m}} = \frac{10}{6\sqrt{3}} = 0.962 mm^2 \tag{48}$$

Having the cross-sectional area of conductors, the diameter of each strand of coil is equal to 1.11 mm, and considering the standard diameter of wires, the cross-sectional area of each conductor is recalculated as 1.13 mm^2. With these new values, the maximum current density is equal to $\delta = 5.12\, A/mm^2$, which is lower than the value of $\delta = 6\, A/mm^2$ and provides the conditions of problem. Therefore, the total cross-sectional area of winding in stator slot is $Na_c = 197.75 mm^2$. If the space coefficient of stator slot is equal to $k_s = 0.6$, the area of each stator slot is obtained from the following equation:

$$a_s = \frac{Na_c}{k_s} = \frac{197.7}{0.6} \approx 329mm^2 \tag{49}$$

The number of turns that are placed horizontally together is considered equal to 11. With this assumption, the number of vertical conductors is equal to 16 rows. Considering 1 *mm* on each side for the stator slot, the width of slot is calculated as follows:

$$W_{ss} = (1.2 \times 11) + 2 = 15.2mm \tag{50}$$

Therefore, the height of stator slot is calculated as follows:

$$h_{ss} = \frac{Na_c}{k_s W_{ss}} = \frac{329}{15.2} = 21.6mm \tag{51}$$

The number of vertical conductors in the stator slot is considered equal to 16. Therefore, the stator slot height is calculated according to the diameter of each conductor $h_{ss} = (1.2 \times 16) + 2 = 21.2mm$, which confirms the considered assumption. Having the stator slot height, the stator tooth height (h_{sp}) is obtained as follows:

$$h_{sp} = h_{ss} + h_{st} = 21.6 + 11.6 = 33.2mm \tag{52}$$

Considering that the STLSRM is three-phase, the stator has 6 teeth and 6 slots. Therefore, the length of stator and the length of translator are obtained as follows:

$$L_s = 6W_{sp} + 6W_{ss} = 182.4mm \tag{53}$$

In (52) and (53) based on sensitivity analysis and for initial design, $h_{st} = 0.35h_{sp}$ and $k_2 = 1$ are considered. In the initial design of motor, $W_{so} = 2W_{os}$ is considered, with this assumption, $W_{os} = 3.8mm$ and then the slot opening $W_{so} = 7.6mm$ is calculated. Therefore, the tip width of stator pole (W_{tsp}) and the upper width of segment (W_{tr}) are calculated as follows:

$$W_{tsp} = W_{sp} + 2W_{os} = 15.2 + 7.6 = 22.8mm \tag{54}$$

$$W_{tr} = 2W_{sp} + W_{os} = 30.4 + 7.6 = 38mm \tag{55}$$

To avoid the phenomenon of local saturation, the stator yoke height (h_{sy}) and the segment height (h_{tr}) are considered equal to the stator pole width. Also, according to the sensitivity analysis, the angle of segment (θ_{tr}) is considered equal to 65° for the initial

design. Finally, using the dimensional equation (27), the axial length of motor (L_{stk}) can be calculated as follows:

$$L_{stk} = \frac{P_o}{\eta V_m ac L_s B_g \frac{1-k_1}{1+k_2}\frac{\tau_s}{\tau_{tr}}} = 135mm \tag{56}$$

where the constant parameters of the dimensional equation are considered as $\eta = 0.5$, $ac = 2500\,A/m$ and $k_1 = 0.33$. The initial design dimensions of the STLSRM are given in Table 1. In the following, with the purpose of reducing the force ripple and increasing the average instantaneous thrust force, optimization is done for the designed STLSRM in next section.

6. Optimization of The Designed STLSRM considering Force Ripple and Average Instantaneous Thrust Force

In this section, in order to reduce the force ripple and increase the average instantaneous thrust force, optimization of the designed STLSRM for the application of electric sliding doors is done based on DOE approach and the RSM. Geometric and control parameters are used as optimization variables. k_2, l_g and θ_{tr} are considered as geometric variables and the turn-on position (x_{on}) and turn-off position (x_{off}) are considered as control parameters. The DOE approach is one of the widely used methods that can be used to identify the key parameters that affect the qualitative characteristics of output. In this statistical method, the input factors can be systematically changed and their effect on the responses can be evaluated. In this paper, the approach of DOE based on the RSM is used to optimize the motor dimensions using design expert (DE) software. The range of geometric parameter changes for better STLSRM performance are estimated using sensitivity analysis, which can be used to get an overview of the effect of geometric parameters on motor performance.

The required tests and changes of each parameter are defined by the DE software, which are presented in Table 2. Each of these experiments is simulated based on the FEM and by electromagnetic transient analysis. Using the characteristics of instantaneous thrust force, force ripple and average instantaneous thrust force prediction and its results are given in Table 2. For optimization analysis, the transformation of response can be written as a function of parameters, and the transformation that has the best correlation with the least deviation from

the real value is suitable. For this purpose, the residual diagram and the diagram of predicted response values in terms of its actual values are used. When the residual plots are normally distributed, the test results are around the estimated values. The diagram of residuals for force ripple and average thrust force is shown in Fig. 11.

For a variable, the difference between the observed value and the predicted value of model is its residual. The residuals represent the error in the model, which is expected to be normally and independently distributed, so that their mean is zero. Therefore, in the normal probability distribution graph for residuals, the curve points are close to the straight line. The accuracy of the model can also be determined by using the graph of predicted responses values from the model in terms of their actual values according to Fig. 11. The closer this graph is to the straight line, the more accurate the model is, and the predicted values are more Conformity with the actual values.

In order to better evaluation of the optimization, the effect of each parameter and the interaction of parameters on the response related to the force ripple and the average thrust force is shown in Fig. 12. In this optimization, the goal is to obtain suitable geometric and control variables in order to optimize the force ripple and the average instantaneous thrust force. Therefore, there is a combination of different factors that the optimization process is done by integrating them.

7. Simulation Results

The design and optimization of a STLSRM for the use of electric sliding doors was done. Simulation results and comparison of initial and optimized designs are presented here. The specifications of initial design and the optimized design with the goal of increasing the average instantaneous thrust force and reducing the force ripple are given in Table 1. The laminations of stator core and moving part are M800-50A with a thickness of 0.5 mm. For the initial design according to the sensitivity analysis, the variables k_2, l_g and θ_{tr} are considered equal to 1, 1 mm and 65°, respectively, while in the optimal design of motor with the design experiments approach and based on the surface response method, these values were calculated 0.96, 0.8 and 52° degrees respectively. For fully aligned and fully unaligned positions, the flux-linkage with one phase for the initial and optimized design of STLSRM for the use of electric sliding doors based on the FEM in the current range of 0 A to 16 A are predicted and the results are shown in Fig. 13.

In Fig. 13, the comparison between the initial design and the optimized design shows that in the optimized design, the difference between aligned and unaligned flux-linkage in all currents is greater than the initial design. Therefore, the co-energy is more in the optimized motor. Having the flux-linkage characteristic for the various currents and different positions of translator, co-energy and static force are obtained from the following equations, respectively [23].

$$w_c(x,i) = \int \lambda(x,i) di \tag{57}$$

$$F(x,i) = \frac{\partial w_c(x,i)}{\partial x} \Big| \underline{i = const} \tag{58}$$

Based on (57), co-energy characteristic for different positions and three current values are obtained, which is depicted in Fig. 14. Based on this figure, the co-energy difference in two positions of aligned and unaligned for the optimized STLSRM is more than the initial design of STLSRM, because the difference between the flux-linkage in aligned and unaligned positions for the optimized design is more than the initial design.

According to (58), the characteristic of static force for different positions and three currents are obtained, which are shown in Fig. 15, and it can be clearly seen that the optimized motor produces more static force due to the co-energy difference. To calculate the dynamic characteristics, including the instantaneous thrust force and the instantaneous current, having the characteristics of the flux-linkage, first, the instantaneous current is obtained from the phase voltage equation as follows [25]:

$$V = Ri + \frac{d\lambda(x,i)}{dt} \tag{59}$$

where R is the resistance of phase winding and V is the phase voltage. Having the static force characteristic and instantaneous current derived from (58) and (59), the instantaneous thrust force and force ripple are calculated. The control parameters for calculating the instantaneous thrust force and force ripple are turn-on position (x_{on}) and turn-off position (x_{off}). For the initial design of motor, x_{on} and x_{off} are considered 3.2 mm and 15.2 mm, respectively, while for the optimized design of the motor, these variables are calculated as 3.85 mm and 15.85 mm, respectively.

Considering these cases, the waveforms of instantaneous thrust force and instantaneous current for designed three-phase motors are shown in Fig. 16 and Fig. 17, respectively. The average instantaneous thrust force and force ripple for the initial design of STLSRM are obtained as 39.92 N and %73.4, respectively, while for the optimized motor, they are calculated as 45.43 N and %67.4, respectively. Therefore, the average instantaneous thrust force for the optimized STLSRM is more than the initial design of STLSRM, and the force ripple has decreased while the maximum instantaneous thrust force has increased. These comparisons show that in the optimized motor, the force ripple has decreased, while the maximum instantaneous thrust force and the average instantaneous thrust force have increased. Also, the RMS value of instantaneous current for the initial design and the optimized design are 4.26 and 4.02, respectively. This comparison shows that in the optimized motor, even though the RMS current is less, more thrust force is produced.

8. Conclusion

Design methods for linear motors are typically performed in the rotary motor domain, then brought back to linear domain with appropriate transformations. The STLSRM has an unusual structure and magnetic circuit, and unlike the conventional LSRM, where the flux passes through both stator yoke and moving part yoke, the flux produced in STLSRM forms an almost circular path around the adjacent poles. Therefore, due to the unusual structure of the STLSRM, the design process of this motor is better to be done in the linear domain. In this paper, a standard and step-by-step design method was described for design of a STLSRM, and it was performed in the linear domain without converting to the rotary domain, which gives the designer more flexibility to choose the appropriate geometric dimensions for the motor and increases the design speed significantly. In this integrated design method, the key and effective parameters on motor performance were investigated and important parameters of motor design were discussed.

Because it is necessary to have sufficient information about the effect of geometric quantities on motor performance, the effect of motor geometric parameters on motor performance was discussed by performing a sensitivity analysis, and detailed and comprehensive instructions were provided for determining motor dimensions using the FEM. After obtaining the design equations and carrying out sensitivity analysis to determine the dimensions of the motor, a STLSRM was designed for the use of electric sliding doors, and with the purpose of reducing force ripple and increasing average instantaneous thrust force, the motor was optimized based on the DOE and RSM. For validation using the FEM, the

performance characteristics of the optimized motor were compared with its initial design. For the current of 12 A, the co-energy difference and the average static force for the initial design were calculated as 5.42 J and 184.73 N, respectively, while for the optimized motor, these values were obtained as 6.59 J and 224.05 N, respectively. To better evaluate the designed motors, the average instantaneous thrust force and force ripple for the initial design of STLSRM were obtained as 39.92 N and %73.4, respectively, while for the optimized STLSRM, they were calculated as 45.43 N and %67.4, respectively. Also, the RMS value of instantaneous current for the initial design and the optimized design were predicted 4.26 A and 4.02 A, respectively. These comparisons showed that the optimized model for the use of sliding doors has a better performance than the initial model.

9. References

[1] Wang, D., Feng, Z., Zheng, H., et al. "Comparative analysis of different topologies of linear switched reluctance motor with segmented secondary for vertical actuation systems", IEEE Trans. Energy Convers. 36(4), pp. 2634–2645 (2021). DOI: 10.1109/TEC.2021.3070563

[2] Davarpanah, G., Faiz, J., and Shirzad, H. "A C-core connected two-phase switched reluctance motor with embedded permanent pagnets for developed torque enhancement", IEEE Trans. Ind. Elect. 71(3), pp. 2332-2342 (2024). DOI: 10.1109/TIE.2023.3269460

[3] Cheng, H., Liao, S., and Yan, W. "Development and performance analysis of segmented-double-stator switched reluctance machine", IEEE Trans. Ind. Electron., 69(2), pp. 1298-1309 (2022). DOI: 10.1109/TIE.2021.3059554

[4] Upadhyay, P. and K, R. "Design of two-phase 4/6 switched reluctance motor for bidirectional starting in washing machine application", IEEE Trans. Ind. App. 59(2), pp. 1519-1529 (2023). DOI: 10.1109/TIA.2022.3221908

[5] Kumar, P., Israyelu, M., and Sashidhar, S. "A simple four-phase switched reluctance motor drive for ceiling fan applications", IEEE Access, 11, pp. 7021-7030 (2023). DOI: 10.1109/ACCESS.2023.3238068

[6] Sun, X., Wan, B., Lei, G., et al. "Multiobjective and multiphysics design optimization of a switched reluctance motor for electric vehicle applications", IEEE Trans. Energy Convers. 36(4), pp. 3294–3304 (2021). DOI: 10.1109/TEC.2021.3078547

[7] Lobo, N. S., Lim, H. S., and Krishnan, R. "Comparison of linear switched reluctance machines for vertical propulsion application: Analysis, design, and experimental

correlation", IEEE Trans. Ind. Appl. 44(4), pp. 1134–1142 (2008). DOI: 10.1109/TIA.2008.926294

[8] Lim, H. S. and Krishnan, R. "Ropeless elevator with linear switched reluctance motor drive actuation systems", IEEE Trans. Ind. Electron. 54(4), pp. 2209–2218 (2007). DOI: 10.1109/TIE.2007.899875

[9] Masoudi, S., Mehrjerdi, H., and Ghorbani, A. "New elevator system constructed by multi- translator linear switched reluctance motor with enhanced motion quality", IET Electr. Power Appl. 14(9), pp. 1692–1701 (2020). DOI: 10.1049/iet-epa.2019.0996

[10] Nie, R., Chen, H., Zhao, W., et al. "Comparative researches on double- sided switched reluctance linear machines with different winding connections", IET Electr. Power Appl. 14(11), pp. 2082–2091 (2020). DOI: 10.1049/iet-epa.2020.0072

[11] Zare Chavoshi, A. and Ganji, B. "Instantaneous thrust control of linear switched reluctance motors with segmental translator", Scientia Iranica, 27(6), pp. 3140-3149. (2020). DOI: 10.24200/sci.2019.51380.2144

[12] Chen, H., Yuan, W., and Wang, Q. "Electromagnetic analysis of flux characteristics of double-sided switched reluctance linear machine", IEEE Trans. Appl. Supercond. 26(4), pp. 1-7 (2016). DOI: 10.1109/TASC.2016.2539215

[13] Ghaffarpour, A., Vatani, M., Kondelagi, M. A. J., et al. "Analysis of linear permanent magnet switched reluctance motors with modular and segmental movers", IET Electr. Power Appl. 17(6), pp. 756–772 (2023). DOI: 10.1049/elp2.12300

[14] Chen, H., Liu, J., Wang, X., et al. "A novel method to suppress the force ripple of a switched reluctance linear motor", IEEE Trans. Ind. App. 58(4), pp. 4792-4803 (2022). DOI: 10.1109/TIA.2022.3177398

[15] Lim, H.S., Krishnan, R., and Lobo, N.S. "Design and control of a linear propulsion system for an elevator using linear switched reluctance motor drives", IEEE Trans. Ind. Electron. 55(2), pp. 534–542 (2008). DOI: 10.1109/TIE.2007.911942

[16] Lee, B., Bae, H., Vijayraghavan, P., et al. "Design of a linear switched reluctance machine", IEEE Trans. Ind. Appl. (36)6, pp. 1571–1580 (2000). DOI: 10.1109/28.887208

[17] Wang, D., Zhang, D., Du, X., et al. "Unitized design methodology of linear switched reluctance motor with segmental secondary for long rail propulsion application", IEEE Trans. Ind. Electron. 65(12), pp. 9884-9894 (2018). DOI: 10.1109/TIE.2018.2829690

[18] Wang, D., Wang, X., Du, X. “Design and comparison of a high force density dual-side linear switched reluctance motor for long rail propulsion application with low cost”, IEEE Trans. Mag. 53(6), pp. 1-4 (2017). DOI: 10.1109/TMAG.2017.2659804

[19] Li, Z., Wang, D., Huang, C., et al. “Nonlinear analytical model of linear switched reluctance motor with segmented secondary considering iron saturation and end effect”, IEEE Access, 11, pp. 132078-132087 (2023). DOI: 10.1109/ACCESS.2023.3335811

[20] Vattikuti, N., Malkani, V.R., and Fernandes, B.G. “A novel high force density linear segmented switched reluctance machine”, 34th Annual Conf. of IEEE Industrial Electronics, Orlando, FL, pp. 1083–1088 (2008). DOI: 10.1109/IECON.2008.4758105

[21] Ganji, B. and Askari, M.H. “Analysis and modeling of different topologies for linear switched reluctance motor using finite element method”, Alex. Eng. J. 55(3), pp. 2531–38 (2016). DOI: 10.1016/j.aej.2016.07.017

[22] Golzarzadeh, M., Oraee, H., and Ganji, B. “Lumped parameter thermal model for segmental translator linear switched reluctance motor”, IET Electr. Power Appl. 17(12), pp. 1–14 (2023). DOI: 10.1049/elp2.12362

[23] Golzarzadeh, M. and Ganji, B. “Analytical modelling of the linear switched reluctance motor with segmental translator”, IET Electr. Power Appl. 13(4), pp. 527–537 (2019). DOI: 10.1049/iet-epa.2018.5516

[24] Naderi, P. and Heidary, M. “A novel permanent magnet flux-switching linear motor performance analysis by flexible MEC method”, IEEE Trans. Energy Convers. 36(3), pp. 1910-1918 (2021). DOI: 10.1109/TEC.2020.3046139

[25] Krishnan, R. “Switched reluctance motor drives: modeling, simulation, analysis, and applications”, CRC Press, Boca Raton, (2001). DOI: 10.1201/9781420041644

Figures:

Fig. 1. A 3-phase segmental translator linear switched reluctance motor**. (a)** Two-dimensional geometry, **(b)** Three-dimensional geometry

Fig. 2. Two important positions for translator**. (a)** Aligned, **(b)** Unaligned

Fig. 3. Required design parameters

Fig. 4. The effect of k_2 on the flux path. **(a)** Aligned position with small k_2, **(b)** Unaligned position with small k_2, **(c)** Aligned position with large k_2, **(d)** Unaligned position with large k_2

Fig. 5. The effect of k_2 on motor performance**. (a)** Inductance, **(b)** Average thrust force

Fig. 6. Dimensions of segment

Fig. 7. The effect of θ_{tr} (W_{trb}) on the flux path. **(a)** Aligned position with large θ_{tr}, **(b)** Aligned position with small θ_{tr}, **(c)** Unaligned position with large θ_{tr}, **(d)** Unaligned position with small θ_{tr}

Fig. 8. The effect of θ_{tr} on motor performance**. (a)** Inductance, **(b)** Average thrust force

Fig. 9. The effect of k_3 on motor performance. **(a)** Inductance, **(b)** Average thrust force

Fig. 10. The effect of l_g on motor performance. **(a)** Inductance, **(b)** Average thrust force

Fig. 11. The graph of residual and the graph of predicted response values in terms of its actual values**. (a)** Force ripple, **(b)** Average instantaneous thrust force

Fig. 12. Interaction of geometric and control parameters on ripple force and average momentary thrust force. **(a)** Force ripple, **(b)** Average instantaneous thrust force

Fig. 13. Flux-linkage with one phase

Fig. 14. Co-energy for various currents and different positions

Fig. 15. Static force characteristic for 3 currents and different positions

Fig. 16. Instantaneous thrust force waveforms for the 3-phase STLSRM**. (a)** Initial design, **(b)** Optimized motor

Fig. 17. Instantaneous current waveforms for the 3-phase STLSRM**. (a)** Initial design, **(b)** Optimized motor

Tables:

Table 1 Specifications of STLSRMs

Table 2 Experiments and simulation responses

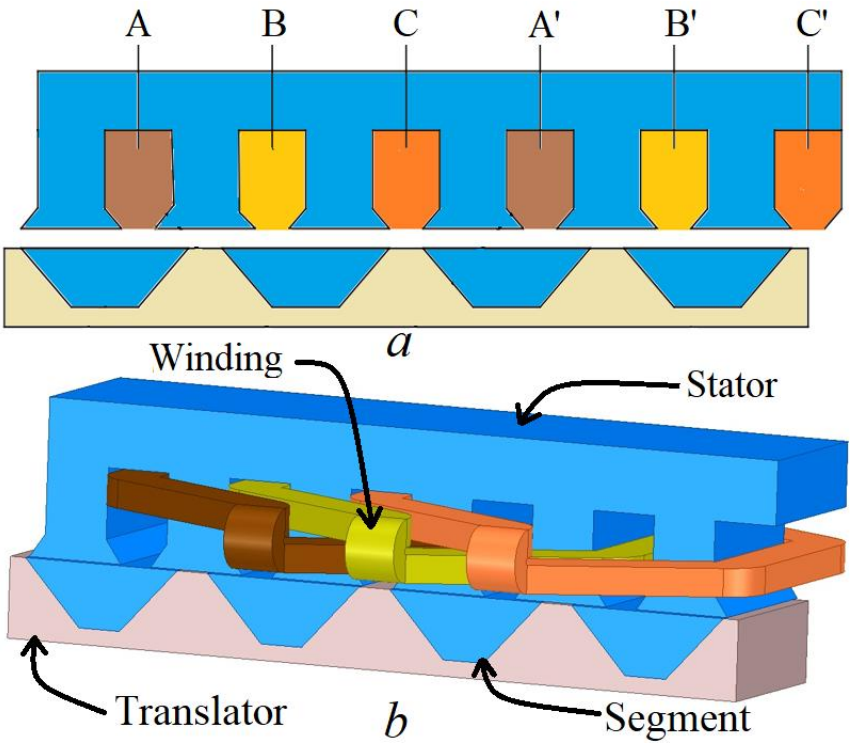

Fig. 1. *A 3-phase segmental translator linear switched reluctance motor*

(a) *Two-dimensional geometry,* ***(b)*** *Three-dimensional geometry*

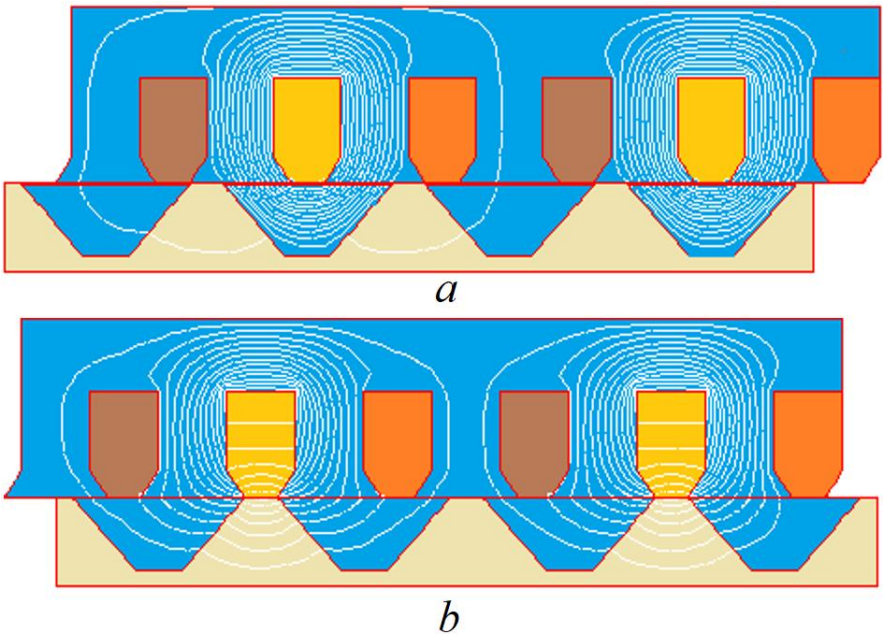

Fig. 2. *Two important positions for translator*

(a) *Aligned,* ***(b)*** *Unaligned*

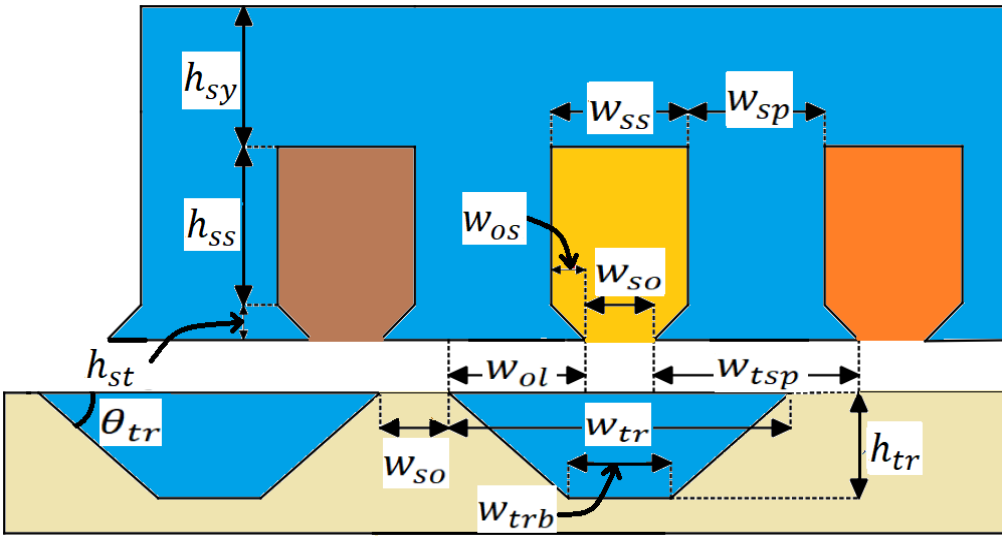

Fig. 3. *Required design parameters*

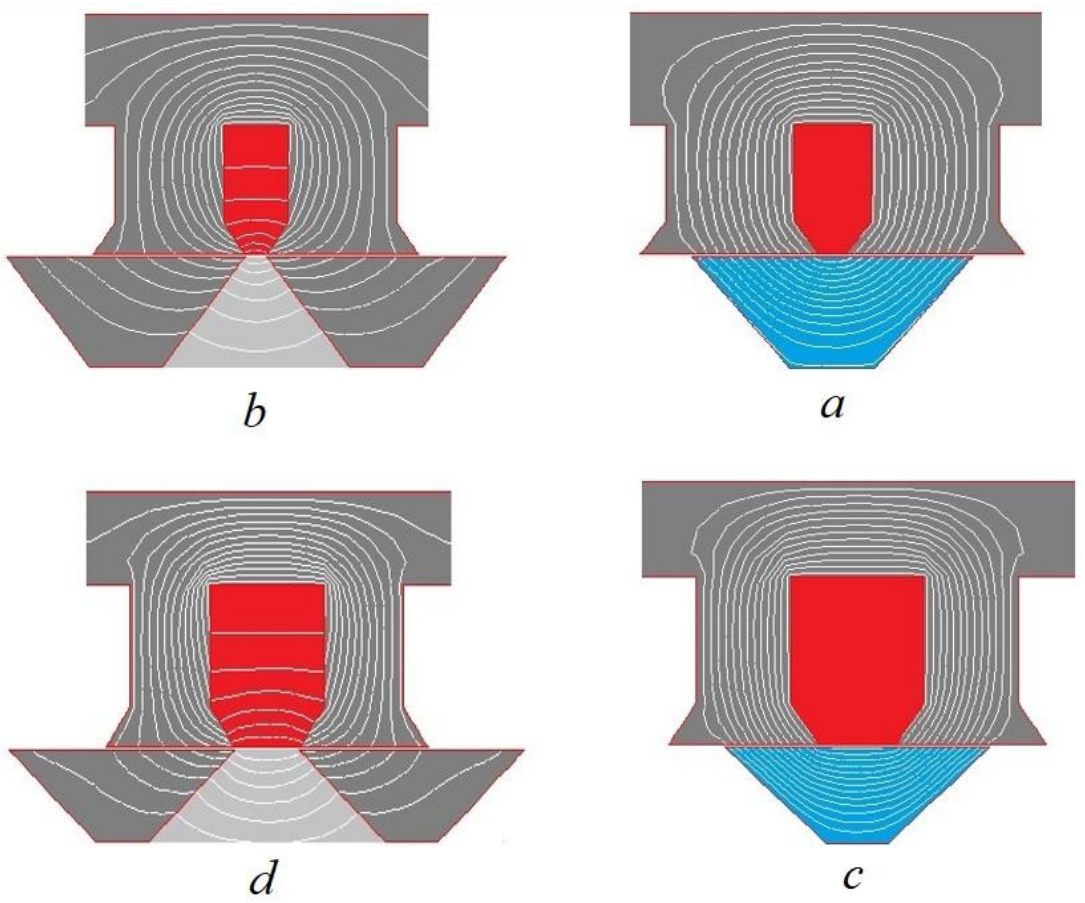

Fig. 4. *The effect of* k_2 *on the flux path,*

(a) *Aligned position with small* k_2, ***(b)*** *Unaligned position with small* k_2, ***(c)*** *Aligned position with large* k_2, ***(d)*** *Unaligned position with large* k_2

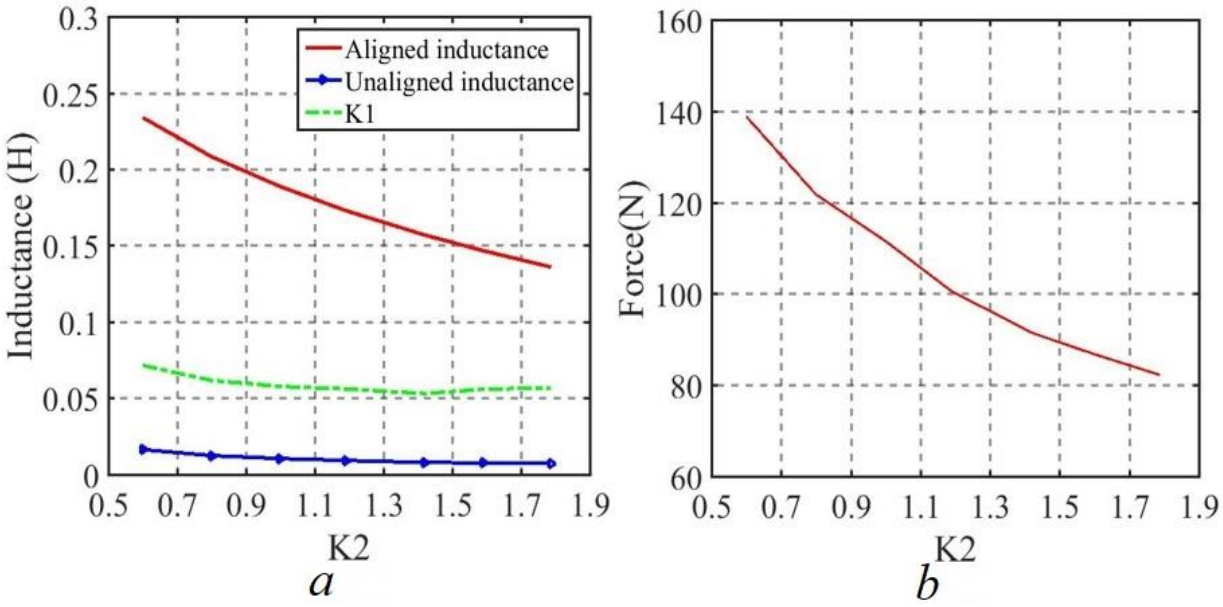

Fig. 5. *The effect of* k_2 *on motor performance*

(a) *Inductance,* ***(b)*** *Average thrust force*

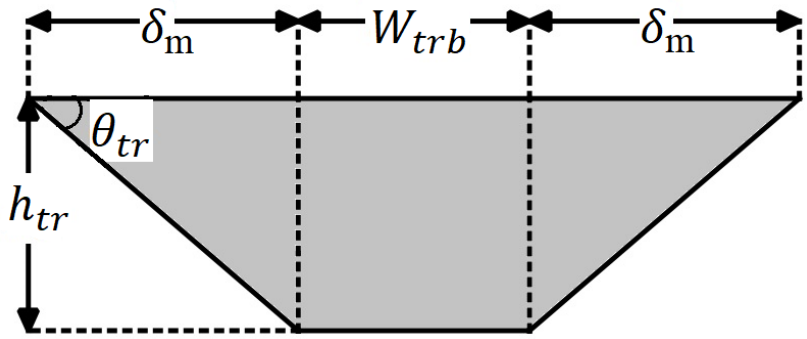

Fig. 6. *Dimensions of segment*

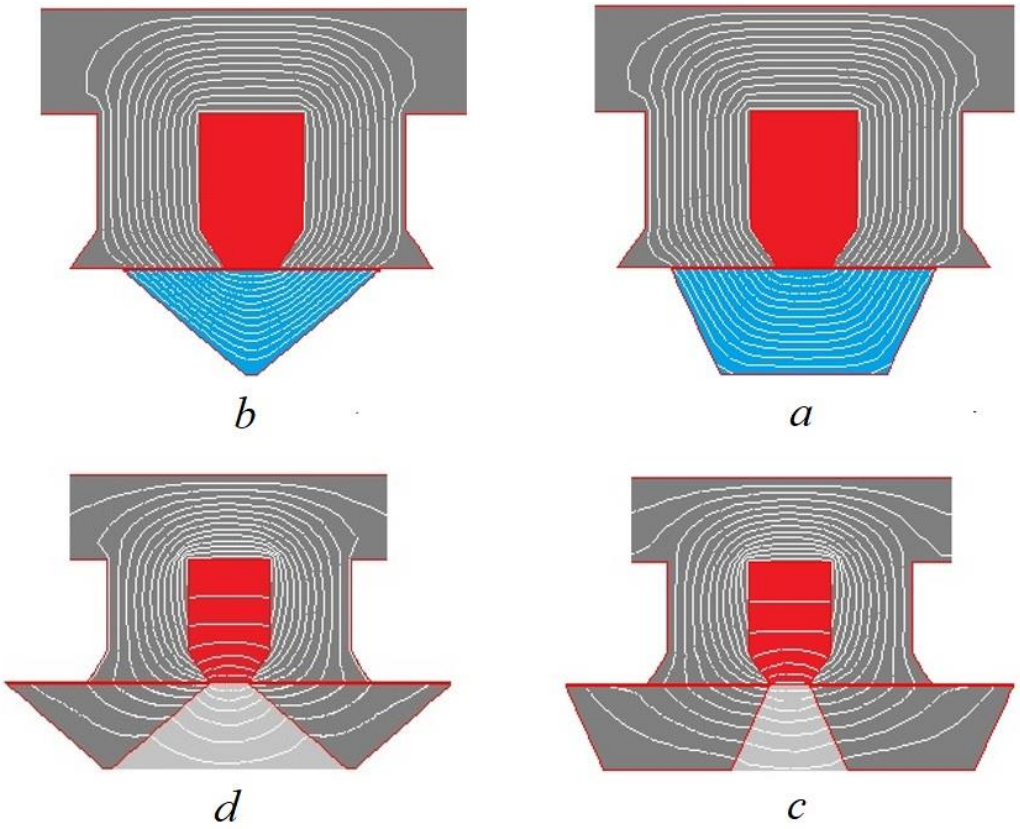

Fig. 7. *The effect of* θ_{tr} (W_{trb}) *on the flux path,*

(a) *Aligned position with large* θ_{tr} *,* ***(b)*** *Aligned position with small* θ_{tr} *,* ***(c)*** *Unaligned position with large* θ_{tr} *,* ***(d)*** *Unaligned position with small* θ_{tr}

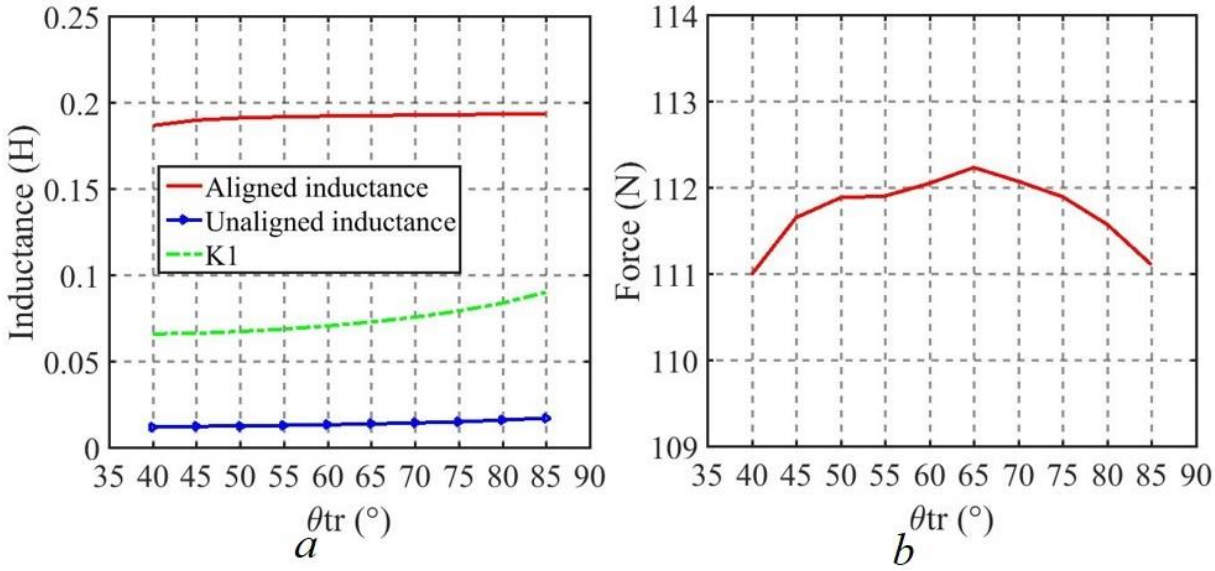

Fig. 8. *The effect of* θ_{tr} *on motor performance*

(a) *Inductance,* ***(b)*** *Average thrust force*

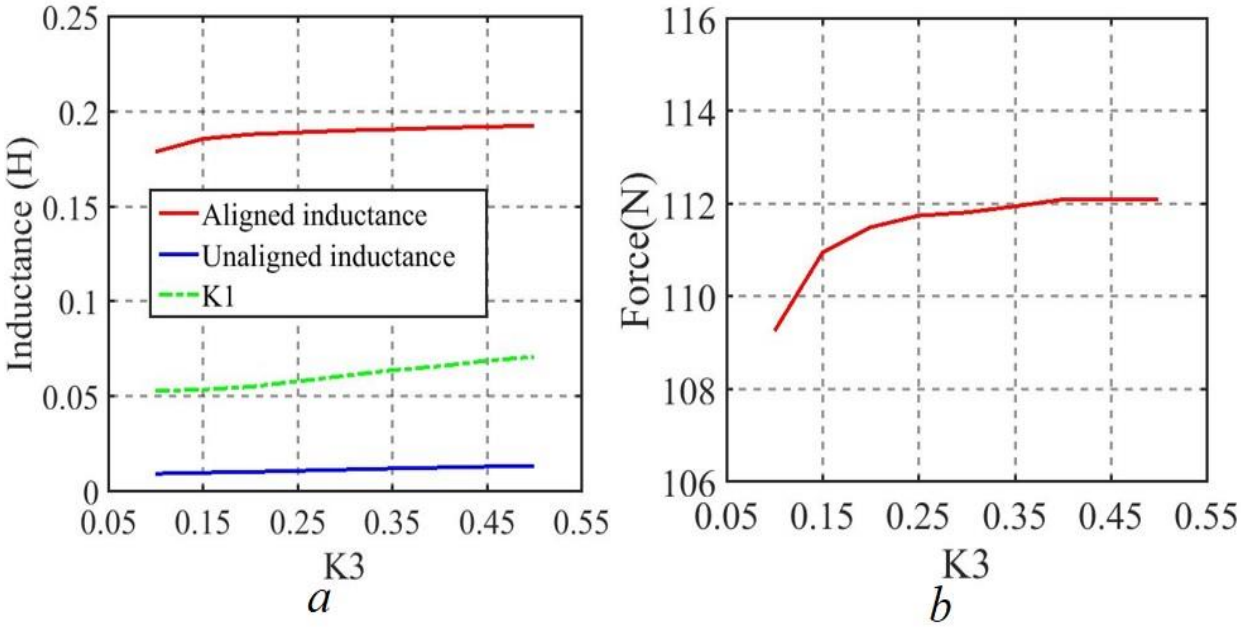

Fig. 9. *The effect of* k_3 *on motor performance,*

(a) *Inductance,* ***(b)*** *Average thrust force*

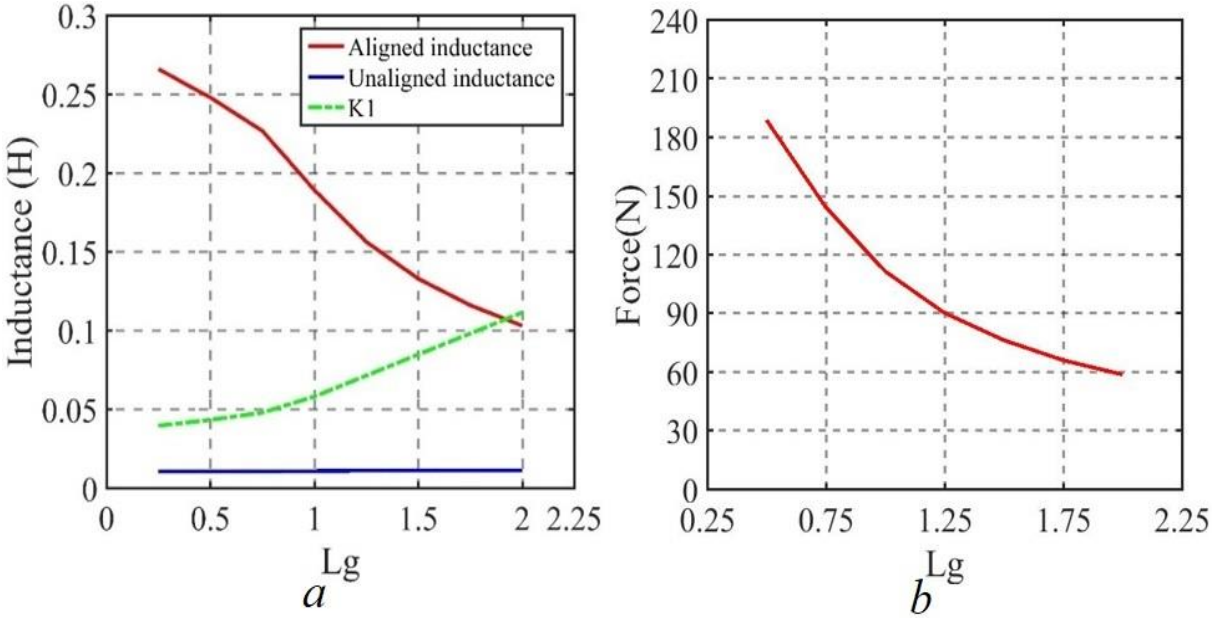

Fig. 10. *The effect of* l_g *on motor performance,*

(a) *Inductance,* ***(b)*** *Average thrust force*

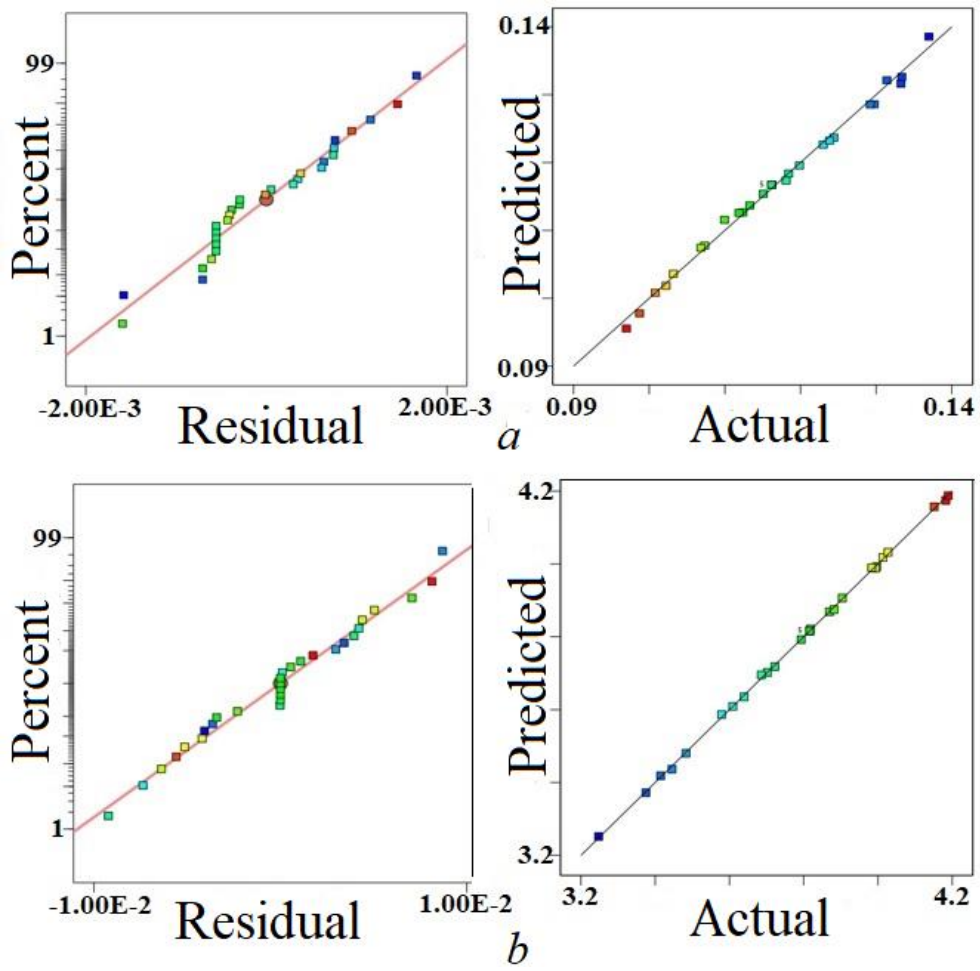

Fig. 11. *The graph of residual and the graph of predicted response values in terms of its actual values*

(a) *Force ripple,* ***(b)*** *Average instantaneous thrust force*

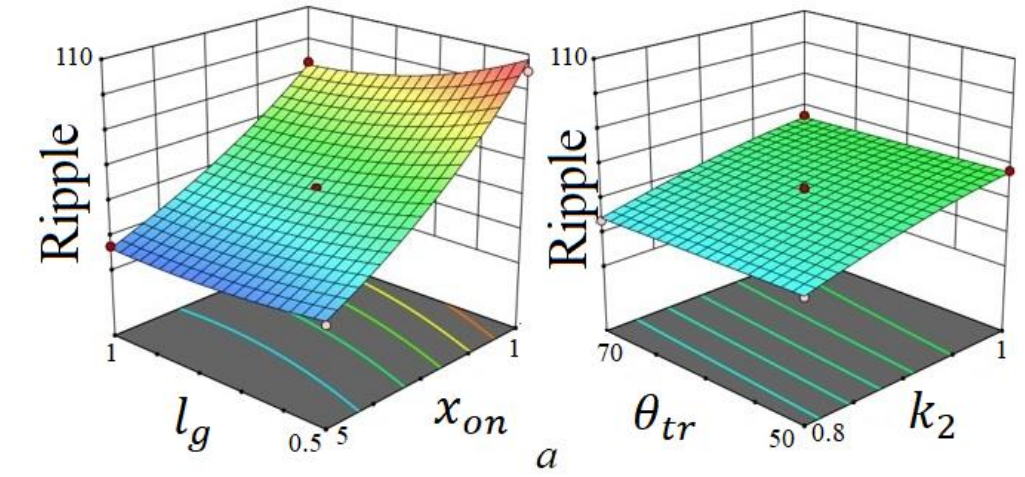

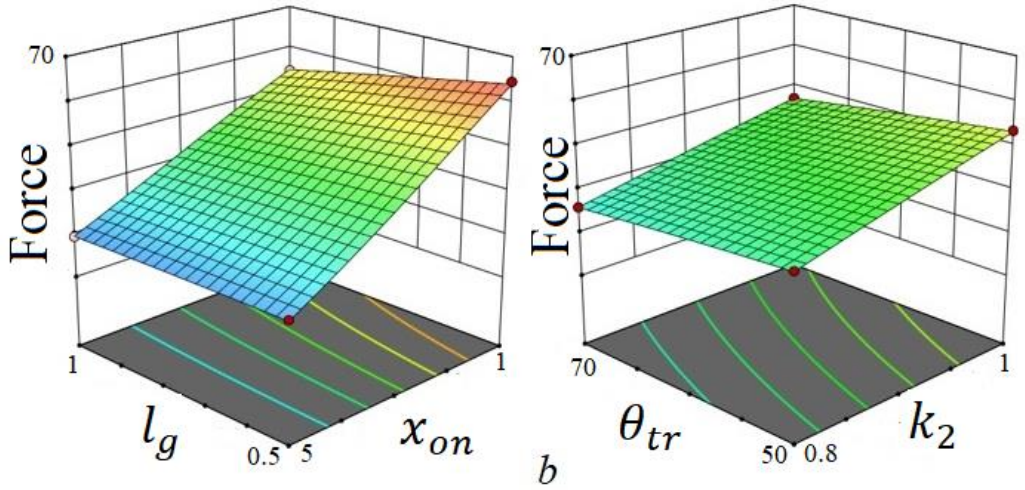

Fig. 12. *Interaction of geometric and control parameters on ripple force and average momentary thrust force*

(a) *Force ripple,* ***(b)*** *Average instantaneous thrust force*

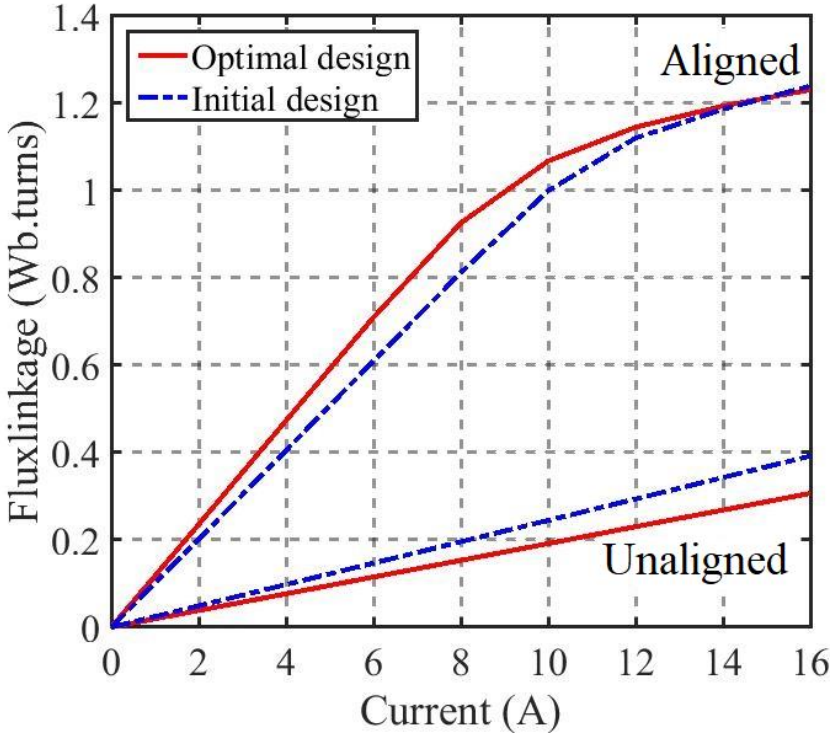

Fig. 13. *Flux-linkage with one phase*

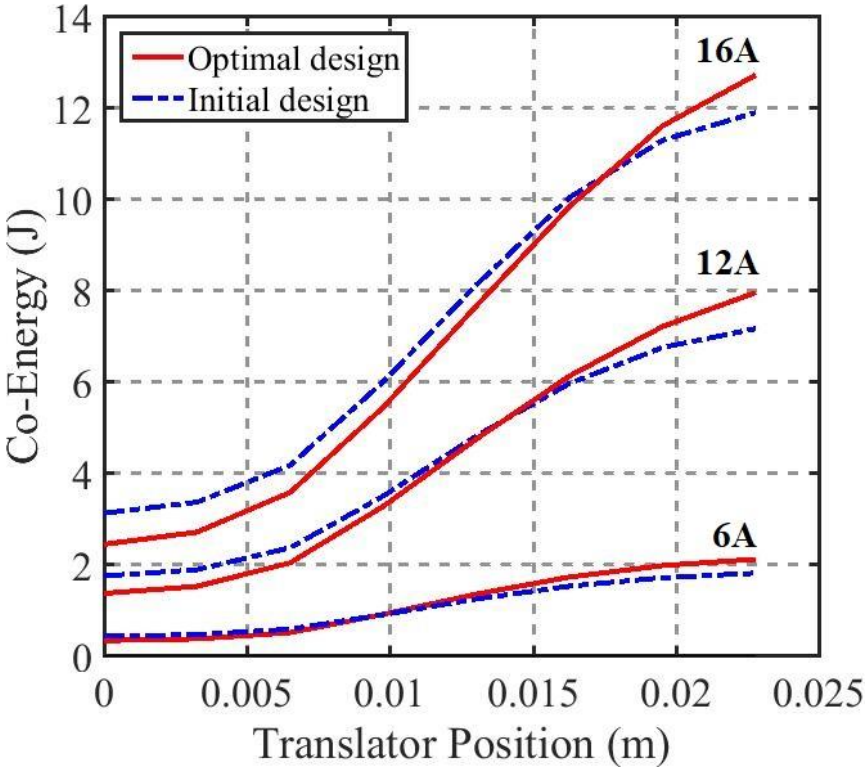

Fig. 14. *Co-energy for various currents and different positions*

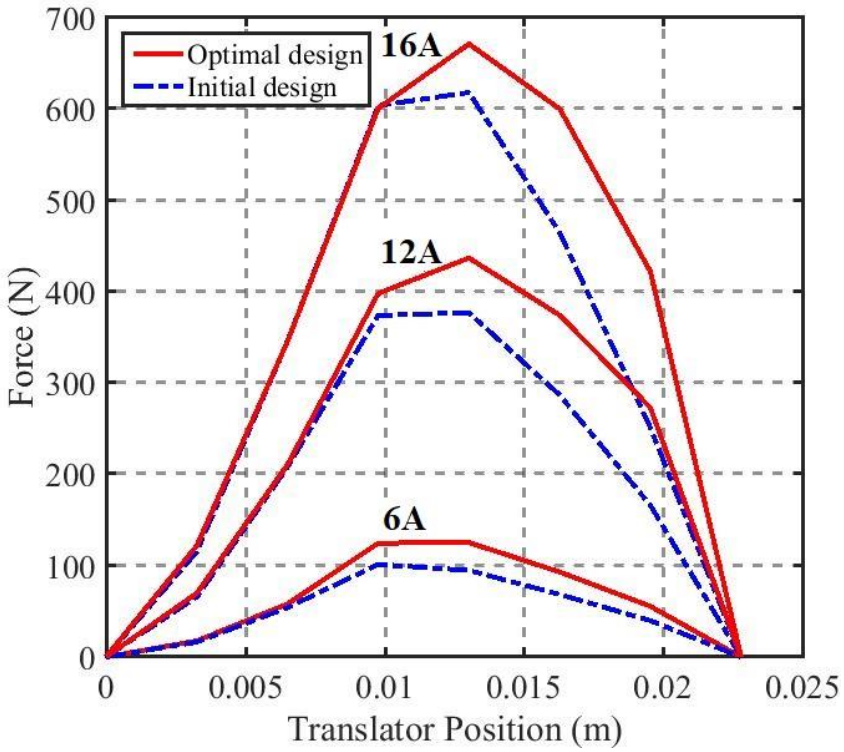

Fig. 15. *Static force characteristic for 3 currents and different positions*

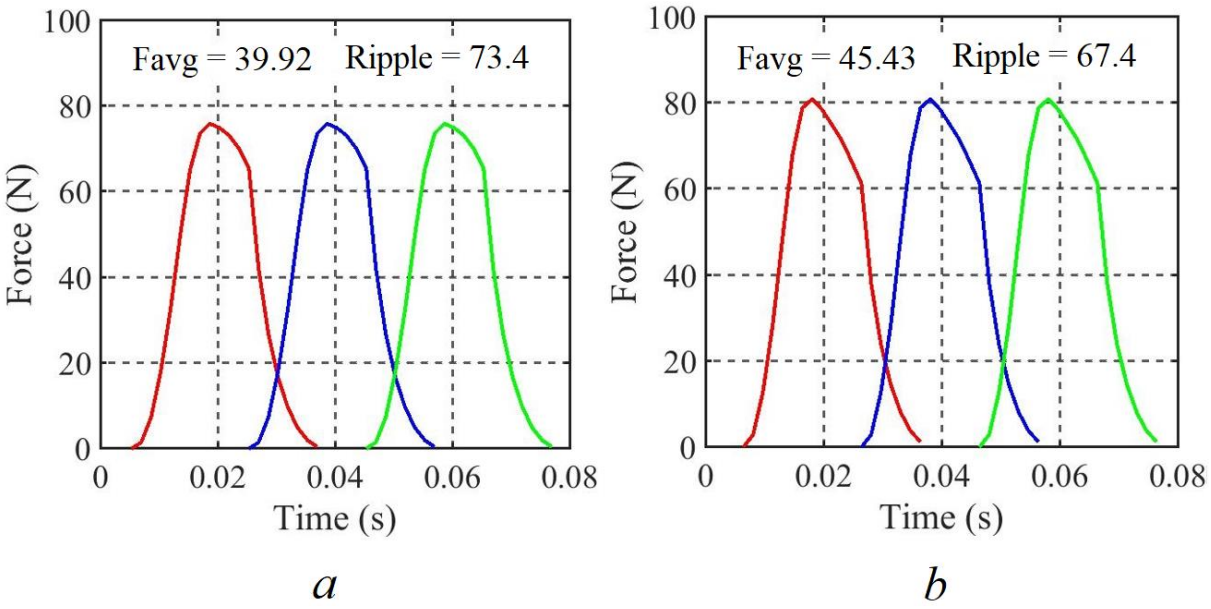

Fig. 16. *Instantaneous thrust force waveforms for the 3-phase STLSRM*

(a) *Initial design,* ***(b)*** *Optimized motor*

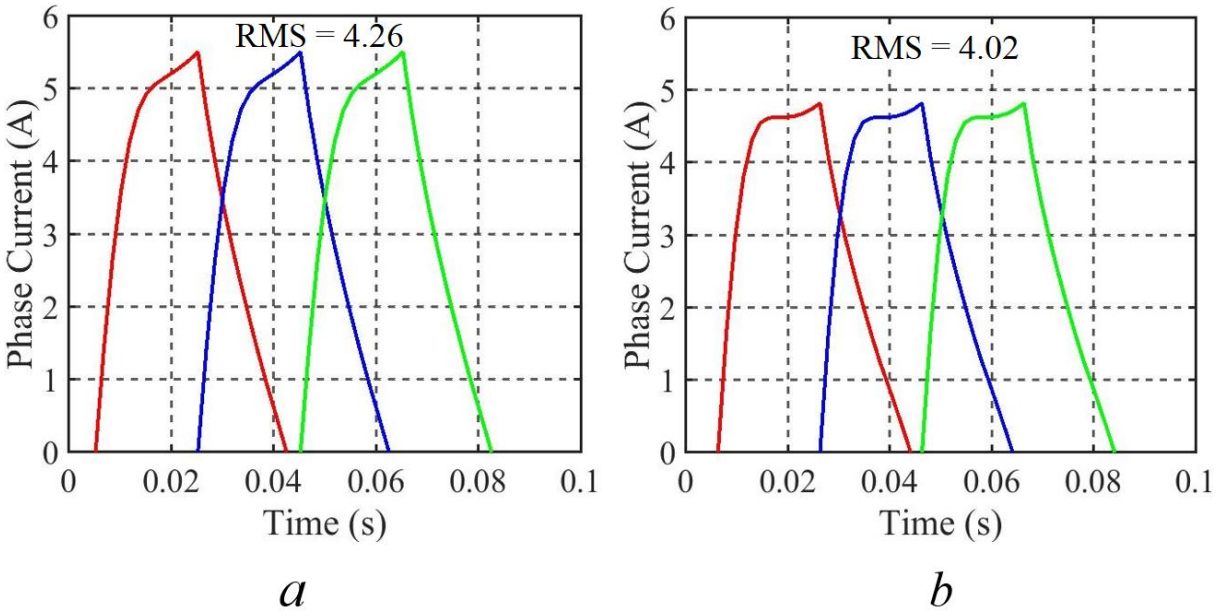

Fig. 17. *Instantaneous current waveforms for the 3-phase STLSRM*

(a) *Initial design,* ***(b)*** *Optimized motor*

Table 1 Specifications of STLSRMs

Parameters	Initial design	Optimized design
Stator pole width [mm]	15.2	15.5
Stator slot width [mm]	15.2	14.9
Stator pole height [mm]	33.2	27
Stator yoke height [mm]	15.2	15.5
Air-gap length [mm]	1	0.8
Segment upper width [mm]	38	38.3
Segment bottom width [mm]	23.82	14.08
slot opening width [mm]	7.6	7.3
Segment height [mm]	15.2	15.5
Core stack thickness [mm]	135	135
Turns per phase	175	175
Resistance [Ω]	0.69	0.69

Table 2 Experiments and simulation responses

No.	k_2	$\theta_{tr}(^{\circ})$	$l_g(mm)$	$x_{on}(mm)$	$R(\%)$	$F_{avg}(N)$
1	0.9	50	0.5	3	81.7	48.6
2	0.9	60	0.75	3	73.1	44.43
3	0.8	70	0.75	3	63.6	35.93
4	0.9	60	0.75	3	73.1	44.43
5	0.9	60	0.5	1	105.3	64.53
6	0.9	60	1	1	92.9	54.34
7	1	60	0.5	3	86.6	52.69
8	0.9	60	1	5	56.92	29.41
9	1	60	0.75	5	58.9	34.84
10	0.9	50	1	3	70.7	44.51
11	0.8	60	0.75	1	85.8	53.22
12	0.9	70	0.75	1	94.7	55.09
13	1	50	0.75	3	78.2	53.43
14	0.9	50	0.75	5	55.3	31.56
15	0.9	70	0.5	3	78.9	43.4
16	0.9	60	0.75	3	73.1	44.43
17	0.9	60	0.5	5	58.4	30.35
18	1	60	1	3	74.5	47.51
19	0.8	50	0.75	3	65.1	40.36
20	1	60	0.75	1	101.6	64.96
21	0.8	60	1	3	64.2	37.07
22	0.9	60	0.75	3	73.1	44.43
23	0.9	50	0.75	1	97.4	62.52
24	0.8	60	0.5	3	68.6	38.88
25	0.9	70	0.75	5	55.2	28.23
26	1	70	0.75	3	76.9	46.91
27	0.8	60	0.75	5	52.3	24.73
28	0.9	60	0.75	3	73.1	44.43
29	0.9	70	1	3	70.3	39.54

Technical Biography of Authors:

Milad Golzarzadeh is currently a PhD candidate in electrical power engineering at Sharif University of Technology, Tehran, Iran. His research interests include modeling and design of electric machines, linear switched reluctance motors, thermal modeling of electric machines, permanent magnet motors and power electronics and drives.

Hashem Oraee (Fellow of IET, Senior Member of IEEE) received the B.Eng. in electrical and electronic engineering from University of Wales, Cardiff, U.K., in 1980, and the Ph.D. degree in electrical machines from the University of Cambridge, Cambridge, U.K., in 1984. He is currently a Full Professor with the Department of Electrical Engineering, Sharif University of Technology, Tehran, Iran. His current research interests include renewable energies, electrical machines, and DFIGs.

Babak Ganji (Senior Member of IEEE) received the B.Sc. degree from Esfahan University of Technology, Iran in 2000, and M.Sc. and Ph.D. from the University of Tehran, Iran in 2002 and 2009 respectively, all in electrical power engineering. He is currently an Associate Professor with the Faculty of Electrical and Computer Engineering, University of Kashan, Kashan, Iran. His research interest is modeling and design of advanced electric machines, especially switched reluctance motor.